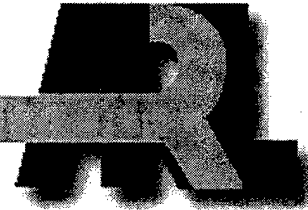


ARMY RESEARCH LABORATORY



A Numerical Investigation of Supersonic Jet Interaction for Finned Bodies

Mary J. Graham
Paul Weinacht
Julius Brandeis
Rick Angelini

ARL-TR-2312

DECEMBER 2000

20010105 120

Approved for public release; distribution is unlimited.

EnSight™ is a trademark of Computational Engineering International, Inc.

INCA® is a registered trademark of Amtec Engineering, Inc.

The findings in this report are not to be construed as an official Department of the Army position
unless so designated by other authorized documents.

Citation of manufacturer's or trade names does not constitute an official endorsement or approval of
the use thereof.

Destroy this report when it is no longer needed. Do not return it to the originator.

Army Research Laboratory
Aberdeen Proving Ground, MD 21005-5066

ARL-TR-2312

December 2000

A Numerical Investigation of Supersonic Jet Interaction for Finned Bodies

Mary J. Graham
United States Military Academy

Paul Weinacht
Weapons & Materials Research Directorate, ARL

Julius Brandeis
Rafael, Israel

Rick Angelini
Computational and Information Sciences Directorate, ARL

Approved for public release; distribution is unlimited.

Abstract

A detailed numerical investigation of the interaction between a lateral jet and the external flow has been performed for a variety of missile body geometries. These include non-finned axisymmetrical bodies and finned bodies with either strakes or aft-mounted tail fins. The computations were performed at Mach numbers 2, 4.5, and 8. To obtain the numerical results, both Reynolds-averaged Navier-Stokes and Euler techniques were applied. The computational results were compared with results from a previously published wind tunnel study that consisted primarily of global force and moment measurements. The results show significant interactions of the jet-induced flow field with the fin surfaces, which produce additional effects compared with the body alone. In agreement with the wind tunnel study, in some cases the presence of lifting surfaces resulted in force and/or moment amplification of the jet interaction with the missile surfaces. The results indicate deamplification of the jet force at Mach 2 for all three bodies. Amplification of the jet force was also observed for high Mach numbers, particularly for the body with strakes. For the results examined here, there were only minor differences in the global force and moment predictions when viscous or inviscid techniques were used. The dependence of the interaction parameters on angle of attack and jet pressure was well predicted by both methods. The numerical techniques showed good agreement with the experiments at supersonic Mach numbers but only fair agreement for the hypersonic, Mach = 8 case.

ACKNOWLEDGMENTS

The experimental data that formed the basis for the computational validation were provided, courtesy of Rafael and the Israeli Ministry of Defense Directorate of Defense Research and Development. Computational resources were obtained through a grant of computer time from the U.S. Army Research Laboratory Major Shared Resource Center through the U.S. Department of Defense (DoD) High Performance Computing (HPC) Modernization Program. Additionally, support for the development and parallelization of the zonal Navier-Stokes flow (ZNSFLOW) code has been made through the DoD HPC modernization computing software support initiative (CHSSI) program.

INTENTIONALLY LEFT BLANK

Contents

1.	Introduction	1
2.	Computational Technique	2
	2.1 Governing Equations	2
	2.2 Navier-Stokes Numerical Technique	3
	2.3 Inviscid Technique	5
3.	Results	6
4.	Scientific Visualization	14
5.	Summary and Conclusions	15
	References	17
	Distribution List	19
	Report Documentation Page	23
	Figures	
1.	Computational Mesh	4
2.	Chimera Gridding Near Jet Nozzle	4
3.	Schematic of Body Geometries	7
4.	Force Amplification Factor Versus Angle of Attack, Mach 2.0, $P_{oj} = 27$ atm, Body Alone and Tail Fins	10
5.	Force Amplification Factor Versus Angle of Attack, Mach 4.5, $P_{oj} = 38$ atm, Body Alone and Tail Fins	10
6.	Force Amplification Factor Versus Angle of Attack, Mach 8, $P_{oj} = 1.9$ atm, Body Alone and Tail Fins	10
7.	Force Amplification Factor Versus Angle of Attack, Mach 2, $P_{oj} = 27$ atm, Strakes	10
8.	Force Amplification Factor Versus Angle of Attack, Mach 4.5, $P_{oj} = 38$ atm, Strakes	11
9.	Force Amplification Factor Versus Angle of Attack, Mach 8, $P_{oj} = 1.9$ atm, Strakes	11
10.	Force Amplification Factor as a Function of Jet Pressure, Mach 4.5, $\alpha = 0^\circ$, Straked Body	12
11.	Force Amplification Factor as a Function of Jet Pressure, Mach 8.0, $\alpha = 0^\circ$, Straked Body	12
12.	Center of Pressure Versus Angle of Attack, Mach 2.0, $P_{oj} = 27$ atm, Body Alone	12
13.	Center of Pressure Versus Angle of Attack, Mach 4.5, $P_{oj} = 38$ atm, Body Alone	12

14.	Center of Pressure Versus Angle of Attack, Mach 8, $P_{oj} = 1.9$ atm, Body Alone	12
15.	Center of Pressure Versus Angle of Attack, Mach 2, $P_{oj} = 27$ atm, Tail Fins	12
16.	Center of Pressure Versus Angle of Attack, Mach 4.5, $P_{oj} = 38$ atm, Tail Fins	13
17.	Center of Pressure Versus Angle of Attack, Mach 8, $P_{oj} = 1.9$ atm, Tail Fins	13
18.	Center of Pressure Versus Angle of Attack, Mach 2, $P_{oj} = 27$ atm, Straked Body	13
19.	Center of Pressure Versus Angle of Attack, Mach 4.5, $P_{oj} = 38$ atm, Straked Body	13
20.	Center of Pressure Versus Angle of Attack, Mach 8, $P_{oj} = 1.9$ atm, Straked Body	14
21.	Jet Interaction Moment as a Function of Angle of Attack, Mach 4.5, $P_{oj} = 38$ atm, Straked Body	14
22.	Jet Interaction Moment as a Function of Jet Pressure, Mach 4.5, $\alpha = 0^\circ$; Straked Body	14

A NUMERICAL INVESTIGATION OF SUPERSONIC JET INTERACTION FOR FINNED BODIES

1. Introduction

The flow field that results from the interaction of a side (lateral) jet injection into a supersonic external flow, called the jet interaction flow field, has been the subject of several experimental [1-5] and numerical [6-11] investigations. The typical jet interaction flow field is complicated because the jet interrupts the oncoming external flow. The qualitative features of the jet interaction flow field include regions of shock-boundary layer interaction and flow separation that have an effect on the overall flow around the body. In our previous work [11], a detailed numerical study was performed for non-finned axisymmetrical bodies. In this paper, results are presented for missiles with several body geometries. The finned missile configurations are body strakes and aft-mounted fins. It was shown previously [11] that for a finless body, deamplification occurred partially because the jet bow shock wrapped around and interacted with the flow underneath the body. The presence of strakes has the effect of blocking the wrap-around phenomenon and channeling the high pressure flow down the body, thereby allowing amplification. The purpose of the current research is to develop a reliable computational capability to assess the performance of control jets and to obtain a quantitative understanding of the flow phenomenon produced by control jets in the presence of strakes and/or fins and to demonstrate that computational fluid dynamics (CFD) simulation is capable of predicting the important features of jet interaction phenomenon.

This report primarily addresses viscous techniques, but we have also examined the ability to use and the feasibility of using inviscid techniques to predict the same forces and moments. Numerical predictions of the supersonic viscous flow have been obtained via an existing Reynolds-averaged Navier-Stokes solver, and the inviscid flow simulations were performed with a three-dimensional (3-D) multi-zone Euler technique. This work demonstrates that numerical techniques are sufficiently mature to be a useful predictive tool in designing jet-control systems and for flow diagnostics that cannot be made in the experiments. Comparisons between viscous and inviscid results can shed new light on the significance of viscous effects (i.e., separation of flow because of shock interaction) in overall vehicle forces and moments.

In addition to the use of several different geometries, the parameters varied in this study are Mach number, angle of attack, and jet stagnation pressure. The Mach numbers are 2.0, 4.5, and 8. The angles of attack range from -10 to 10 degrees. The jet stagnation pressure varies from 3.6 psi to 72 psi. This report

shows that the numerical results corroborate the experimental findings, in which the presence of strakes caused large control force amplification. This permits the use of smaller control jets and therefore results in propellant volume and weight savings.

In the present study, numerical approaches have been applied to investigate the jet interaction phenomena for flight bodies that have lifting surfaces with a single lateral jet in supersonic flight and to demonstrate the advantages to force amplification factor in the presence of these surfaces. An overset grid approach has been applied to more easily resolve the geometry and flow physics associated with the jet interaction problem. All the numerical results have been validated via global force and moment data from a recently published experimental investigation [5].

2. Computational Technique

2.1 Governing Equations

The nonreacting compressible viscous flow, which obeys the Newtonian law of friction about a flight vehicle, is governed by the equations of mass, momentum, and energy conservation, i.e., the Navier-Stokes equations. For these computations, the complete set of 3-D, time-dependent, generalized geometry, Reynolds-averaged, thin layer, Navier-Stokes equations for generalized coordinates ξ , η , and ζ are used and can be written as follows [12]:

$$\frac{\partial \hat{q}}{\partial t} + \frac{\partial \hat{E}}{\partial \xi} + \frac{\partial \hat{F}}{\partial \eta} + \frac{\partial \hat{G}}{\partial \zeta} = \frac{1}{\text{Re}} \frac{\partial \hat{S}}{\partial \zeta}. \quad (1)$$

$\xi = \xi(x, y, z, t)$, $\eta = \eta(x, y, z, t)$, and $\zeta = \zeta(x, y, z, t)$ are the longitudinal coordinate (direction along the body), the circumferential coordinate (direction around the body), and the nearly normal coordinate (outward direction from the body surface), respectively.

The inviscid flux vectors \hat{E} , \hat{F} , and \hat{G} , and the viscous term \hat{S} are functions of the dependent variable $q^T = (\rho, \rho u, \rho v, \rho w, e)$. The inviscid flux vectors and the source term are shown next. Details of the thin layer viscous term are available in the literature.

The local pressure is related to the dependent variables by applying the ideal gas law:

$$p = (\lambda - 1) \left[e - 0.5 \rho (u^2 + v^2 + w^2) \right] \quad (2)$$

in which γ is the ratio of specific heats. Density, ρ , is referenced to ρ_∞ and the total energy, e , to $\rho_\infty a_\infty^2$.

The form of the mass-averaged Navier-Stokes equations requires a model for the turbulent eddy viscosity. There are numerous approaches for determining the turbulent viscosity. The turbulent contributions are supplied through the algebraic two-layer eddy viscosity model developed by Baldwin and Lomax [13], which is patterned after the model of Cebeci [14].

2.2 Navier-Stokes Numerical Technique

The time-dependent Navier-Stokes equations are solved via a time-iterative solution technique to obtain the final steady state converged solution. The particular time-marching technique applied here is the implicit, partially flux-split, upwind numerical scheme developed by Steger et al. [15, 16] and is based on the flux-split approach of Steger and Warming [17]. This scheme employs central differencing in the normal and circumferential directions, η and ζ , respectively, and flux splitting in the stream-wise direction, ξ .

2.2.1 Chimera Composite Overset Structured Grids

To more easily model the geometry and resolve the flow physics associated with the lateral jet problem, the Chimera composite overset grid technique has been applied. The Chimera technique is a domain decomposition approach that allows the entire flow field to be meshed into a collection of independent grids, in which each piece is gridded separately and overset into a main grid. In current computations, the flight body with lateral jet was subdivided into three distinct grids: one for the body, one adjacent to the jet, and one for the jet nozzle. Overset grids are not required to join in any special way. Usually, a major grid covers the main domain (the external flow field about the projectile), and minor grids are generated to resolve the rest of the body or sections of the body (the jet and the nozzle regions).

Figure 1 displays the computational mesh, showing the main grid for the projectile body along with an overset grid to better capture the physics of the jet interaction with the external flow. The overset jet grid is seen here residing on top of the jet exit as a cylinder with a radius larger than the jet nozzle opening itself. A third grid, used to model the jet nozzle, resides underneath the jet grid. The communication between the nozzle grid and the jet grid is point-to-point zonal, however. Figure 2 is a "close-up" of the grid near the jet port, which is covered by the nozzle grid and jet grid. It also shows the Chimera grid for the jet and the projectile body.

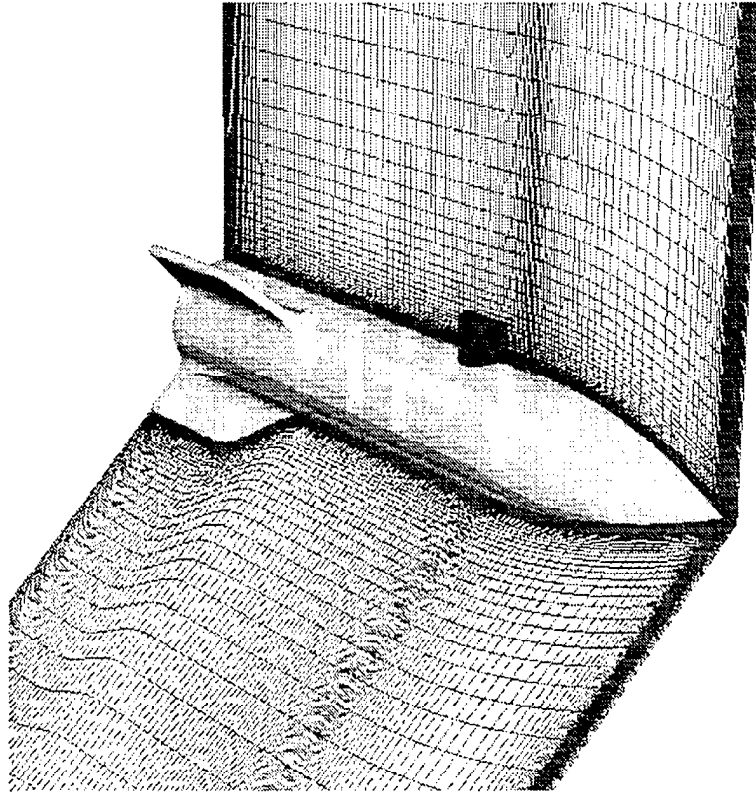


Figure 1. Computational Mesh.

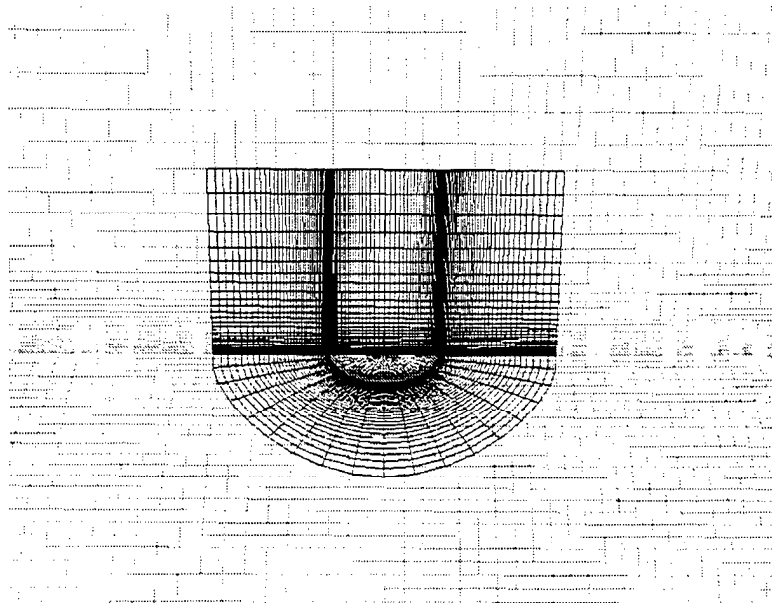


Figure 2. Chimera Gridding Near Jet Nozzle.

2.2.2 Grid Refinement and Computational Time

The baseline computational grid used to generate the published results consisted of approximately 1.6 million points: 153 by 93 by 70 for the projectile (background) grid in the longitudinal, circumferential, and normal directions, respectively; 65 by 21 by 50 for the cylindrically shaped jet grid in the radial, circumferential, and normal directions, respectively; and 25 by 21 by 21 for the nozzle grid in the radial, circumferential, and normal directions. The computational mesh employed a mirror plane of symmetry in the circumferential direction. A grid refinement study was performed to assess grid convergence for the baseline computational grid. Coarse grid solutions were obtained with 115 by 107 by 58, 49 by 16 by 38, and 19 by 16 by 16 grids for the projectile, jet, and nozzle meshes, respectively. Fine grid solutions were obtained with 189 by 167 by 84, 78 by 25 by 60, and 30 by 25 by 25 grids for the projectile, jet, and nozzle meshes, respectively.

Comparisons were made of the forces, moments, amplification factor and center of pressure shift. For the finer grid, there is a 1.1% difference in the jet interaction force and a 1% difference in the moments, amplification factor, and the center of pressure shift. For the coarser grid, there is a 1.2% difference in the jet interaction force and a 1.1% to 2.0% difference in the moments, amplification factor, and the center of pressure shift.

A complete simulation on the baseline grid took approximately 250 central processing unit (CPU) hours on a Silicon Graphics, Inc. (SGI) Origin 2000. The solutions were run in parallel with eight processors, and a parallel acceleration of 5.4 was obtained.

2.3 Inviscid Technique

The flow field solution is obtained here by running the CFD code named INCA[®] [22]. The code is presently run in the Euler (inviscid) mode, but INCA[®] is a multi-block, Navier-Stokes solver with broad capabilities. The field equations are solved via an implicit finite volume method. The evaluation of the inviscid terms is based on flux splitting in combination with upwind biasing.

The numerical solution was run until convergence was reached. The degree of convergence of the solution was judged from the maximum field residue occurring at each time step for each block. In general, convergence level is different in each block, especially for cases with jet activation.

Convergence level is indicated by the logarithm of the largest residual (root mean square, averaged for the field variables). At Mach = 4.5, for the configuration without the jet, convergence of the maximum residual to 10^{-13} was obtained in fewer than 1000 iterations for each of the four blocks. For a typical "jet-on" case, convergence to levels better than 10^{-18} is achieved within 1000

cycles. The convergence properties of the Mach = 8 solutions were very similar to those described for the Mach = 4.5 solutions. From the point of view of integral parameters, such as forces and moments obtained from pressure integration, there is no variation after the residual decreased three or four orders of magnitude.

2.3.1 Computational Grid Generation

The grid is divided into four blocks. This is the minimum number of blocks needed to cover the given topology. The final grid topology used in the inviscid computation of the flow field over the configuration without the jet has about 70,000 grid points. The grid available at this stage is of sufficient resolution for numerical computation of inviscid (Euler) flow about the described missile configuration when the jet is not activated. The jet nozzle has a diameter of 0.5 cm, which is comparable in size to one finite difference cell. To obtain better resolution, local grid refinement in the vicinity of the jet nozzle was performed off line, and the number of grid points defining the nozzle has been quadrupled. Away from the body surface, the grid becomes coarser. Although this will affect the definition of shocks (the shocks are formed of several grid points, which when far apart will give smeared and wavy appearance), the solution close to the body surface will not be affected in the supersonic calculations. The refined grid, giving good definition of the nozzle size and location, consists of about 120,000 points. The block structure described earlier is retained.

2.3.2 Grid Refinement Study (grid independence)

For the configuration presented here, the "jet-off" case was computed with and without the local grid refinement performed to better resolve the area containing the nozzle and the wings' leading edges (120,000 points versus 70,000 points). No difference in solution was observed within plotting accuracy. Grid sensitivity analyses were performed for a prototype configuration, different from the present configuration only in some dimensions. For that configuration (not presented), several grids were used, the finest being coarser than the unrefined grid used in the present report. The graphical results for two successive grids were indistinguishable.

3. Results

Validation of the computational approach for the jet interaction problem was accomplished by a comparison of the predictions with data from a previously published wind tunnel investigation [5]. Supplemental experimental results for the validation were provided courtesy of Rafael and the Ministry of Defense, Directorate of Defense Research & Development. The experiments were conducted at the Israeli Aircraft Industries (IAI) trisonic wind tunnel facility at

Mach numbers of 2 and 4.5 and in the IAI hypersonic wind tunnel facility at Mach 8. While the experimental investigation was quite extensive in scope, the current computational study focused on normal jet injection from a single nozzle geometry at Mach 2, 4.5, and 8. Five different configurations were examined in the experimental study; this report examines three. Global force and moment comparisons were made to validate the computational approach.

Figure 3 shows the three body geometries addressed in this study. Each of the models used has a sharp, ogive-shaped nose section of 2 calibers and a cylindrical afterbody of 3.8 calibers mounted on the midsection for a total length of 5.8 calibers. The reference diameter of the models was 50 mm. For all three geometries, the jet nozzle was 2.5 calibers down stream from the nose tip. A single 5-mm circular nozzle that was designed to achieve sonic flow at the exit was examined here, although additional geometries were considered in the experiment. The strake and aft-mounted fins have the same exposed semi-span of 25 mm and leading edge sweep angle of 45 degrees. Configuration 1 is an axisymmetrical body-alone configuration used as a reference configuration for comparison. Configuration 2 has an aft-mounted tail fin. The root leading edge of each tail surface is 220 mm from the nose tip. Configuration 3 contains strakes spanning 65% of the body's length. The root leading edge is 100 mm from the nose tip. Global force and moment wind tunnel experiments were performed on these bodies.

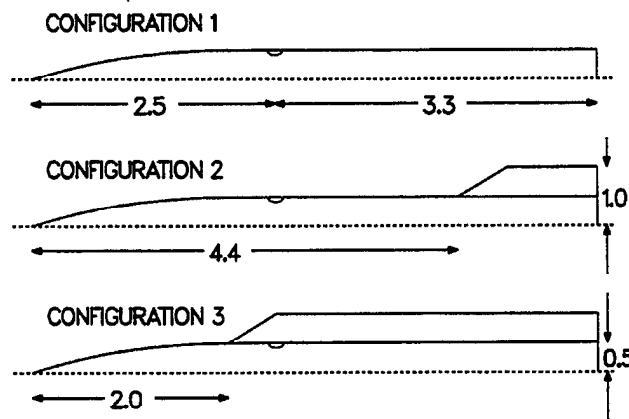


Figure 3. Schematic of Body Geometries.

For the jet interaction problem, the total force acting on the body can be decomposed into three components: the aerodynamic force on the external body in the absence of the jet, the force produced at the jet exit, and the aerodynamic interaction force produced by the jet with the external flow field. In this work, the aerodynamic force on the external body is typically produced when the body is at an angle of attack with the free stream flow. The force produced at the jet exit results from a combination of the momentum flux through the jet nozzle and the integrated pressure at the jet exit. Given that the exit conditions for the jet are

fixed as a boundary condition for the computations, this force component can be explicitly calculated before the flow field computation. The third force component accounts for the force produced by the interaction of the jet with external flow field.

The relationship of these three force components to the total force, F , can be described by the following equation, in which F_{no_jet} is the force in the absence of the jet, F_j is the force produced at the jet exit, and F_{ji} is the jet interaction force:

$$F = F_{no_jet} - (F_j + F_{ji}) \quad (3)$$

The negative sign associated with the two jet forces results because the jet exit hole is situated on the upper surface of the body in the current study and produces a downward force when activated. The jet-off force component typically produces an upward force for positive angles of attack. Note that a positive value of F_{ji} indicates that the interaction force produces an effect that augments the jet force F_j , while a negative value of F_{ji} indicates a reduction in the total force produced by the jet. The jet interaction force accounts for the complete interaction produced by the jet with the external flow field and may vary with angle of attack and jet mass flow rate.

The relative magnitudes of the jet force and the jet interaction force can be compared through a jet interaction amplification factor, K , as shown in Equation 4:

$$K = \frac{F_j + F_{ji}}{F_j} \quad (4)$$

An amplification factor greater than 1 indicates that the jet interaction force amplifies or increases the total force produced by the jet, while an amplification factor small than 1 indicates that the jet interaction force reduces the total force produced by the jet.

In addition to the jet interaction forces, the interaction moments were calculated. In the present case, the center of moments is taken to be the center of the jet nozzle, the assumed center of gravity. The moments considered are pure interaction moment effects which are calculated as follows:

$$\Delta C_m = C_{m_{jet-on}} - C_{m_{jet-off}} \quad (5)$$

in which $C_{m_{jet-on}}$ is the moment coefficient for the configuration with the jet and $C_{m_{jet-off}}$ is the moment coefficient for the configuration without the jet.

The moment interaction can also be assessed by the examination of the center of pressure shift produced by the interaction. The center of pressure shift in calibers is defined as follows with a positive center of pressure shift indicating a rearward movement or a corresponding nose-down pitching moment.

$$\Delta X_{CP} = \frac{-\Delta C_m}{C_{N_j} + C_{N_{ji}}} \quad (6)$$

Figures 4 through 6 display the variation of the force amplification factor with angle of attack at Mach 2, 4.5, and 8 for the body alone and body with tail fins. This comparison is meaningful because ahead of the tail fins (for these supersonic flow cases), the force amplification is essentially identical for both bodies. The differences in the force amplification factor occur only over the aft 1.4 calibers of the body that contain the fins. The predicted results at Mach 2 and 4.5 show excellent agreement with experiment between -10 and 10 degrees angle of attack. At Mach 8, the results show an under-prediction of the jet amplification factor, although the trend with angle of attack is consistent with the experimental data.

The results for the body with tail fins show an increasing trend with angle of attack. For positive angles of attack, the force amplification factor for the tail fins is similar in magnitude to the body-alone results. However, at negative angles of attack, the body with tail fins shows a much stronger deamplification than for the body alone. The differences in the behavior at positive and negative angles of attack are attributable to an interaction of the jet wake on the tail fins. At positive angles of attack, the jet wake is directed away from the tail fins, while at negative angles of attack, the jet wake is convected downward onto the tail fins, thus producing a stronger interaction and deamplification. Ahead of the tail fins, the distribution of the jet interaction force is identical to the body-alone results. Very little additional interaction over the tail fins is seen at $\alpha = 10^\circ$. However, at $\alpha = -10^\circ$, there is a significant interaction over the tail fins, which results in deamplification.

An increasing trend in force amplification factor is noted with increasing Mach number in Figures 4 through 6. However, the force amplification factor also varies with jet pressure. No attempt to scale the jet pressure has been made for the results presented in Figures 4 through 6.

Figures 7 through 9 display the variation of the force amplification factor with angle of attack at Mach 2, 4.5, and 8 for the straked body. At Mach 2 and 4.5, the results are in good agreement with the experimental data across the range of angles of attack. At Mach 8, the computed results do not compare as well with the experimental data. At Mach 4.5 and Mach 8, results were obtained with an inviscid code, as well as with the Navier-Stokes code. At Mach 4.5, there is very

little difference in the predicted results with either code. Similar results are found at Mach 8, where both codes show a trend that is different than the experimental data. The similarity between the predicted results is significant, considering the results were obtained with different codes and computational grids.

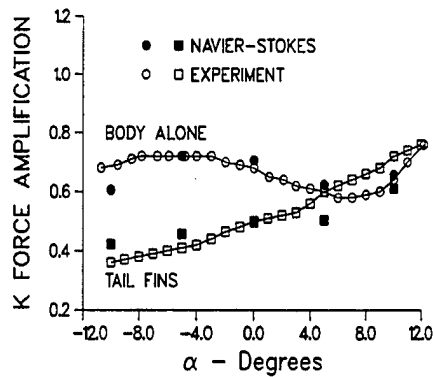


Figure 4. Force Amplification Factor Versus Angle of Attack, Mach 2.0, $P_{o1} = 27\text{atm}$ ¹, Body Alone and Tail Fins.

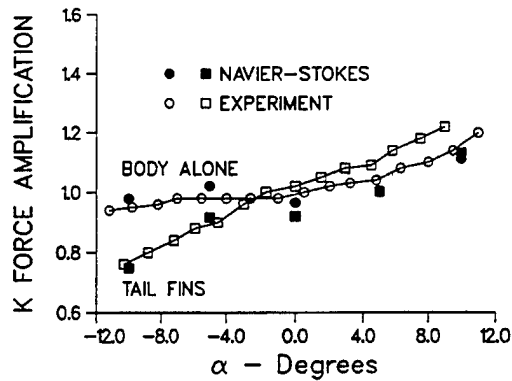


Figure 5. Force Amplification Factor Versus Angle of Attack, Mach 4.5, $P_{o1} = 38\text{atm}$, Body Alone and Tail Fins.

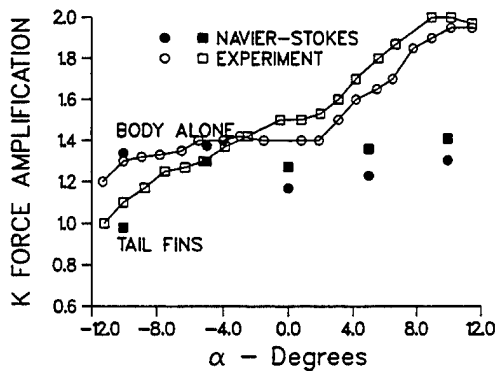


Figure 6. Force Amplification Factor Versus Angle of Attack, Mach 8, $P_{o1} = 1.9\text{atm}$, Body Alone and Tail Fins.

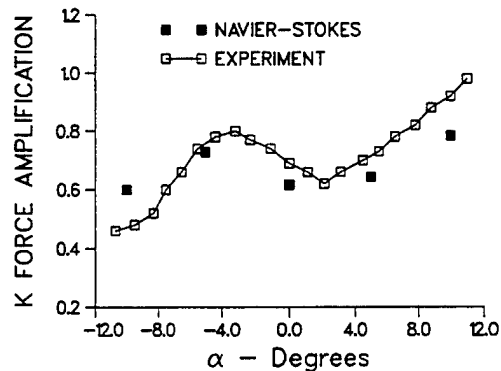


Figure 7. Force Amplification Factor Versus Angle of Attack, Mach 2, $P_{o1} = 27\text{atm}$, Strakes.

A comparison of the jet interaction force distribution was performed for the body alone and the body with strakes at 0 degrees angle of attack at Mach 2, 4.5, and 8. For all three Mach numbers, the presence of the strakes amplifies the jet interaction effect. Near the jet exit, the high pressure behind the jet bow shock acts not only on the body but on the adjacent fins as well. This produces an additional force augmentation relative to the body alone. At Mach 2, the effect of the low pressure region behind the jet is also increased for the straked body, thus producing a force component that results in a deamplification of the jet force.

¹atm = atmospheres

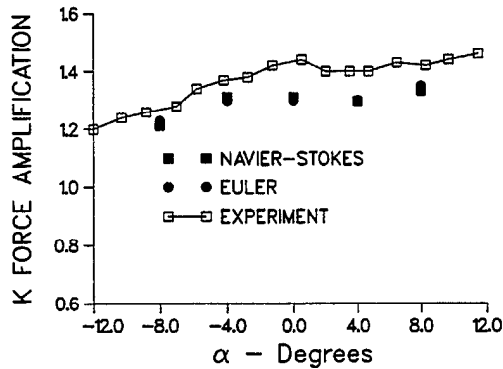


Figure 8. Force Amplification Factor Versus Angle of Attack, Mach 4.5, $P_{0j} = 38$ atm, Strakes.

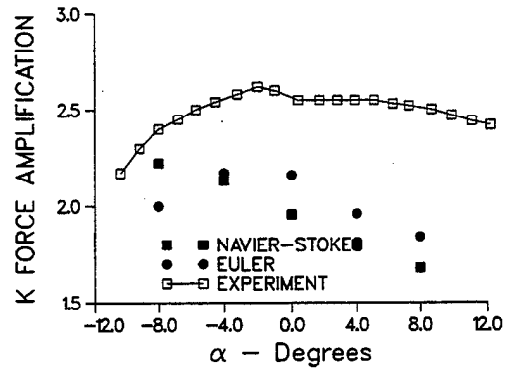


Figure 9. Force Amplification Factor Versus Angle of Attack, Mach 8, $P_{0j} = 1.9$ atm, Strakes.

The force amplification factor for the straked body also shows an apparent increasing trend with Mach number as did the results for the body alone and body with tail fins shown previously. Again, it may be difficult to draw a general conclusion from these results alone because of the dependence of the amplification factor on jet pressure. Figures 10 and 11 show the variation of the force amplification factor with jet pressure at zero degrees angle of attack for Mach 4.5 and 8, respectively. The force amplification factor for both Mach numbers decreases with increasing jet pressure because the force attributable to the jet increases faster than the jet interaction force. The sharp decreasing trend in force amplification as jet pressure increases is captured by both the inviscid and viscous simulations. At Mach 4.5, it is seen that the predicted force amplification factor as a function of jet pressure exhibits the same quantitative variation as the experiment, slightly under-predicting the magnitude. The computed results at Mach 8 have the same qualities as the experiment but under-predict the magnitude. It was anticipated that a viscous code would close the gap between the Euler code predictions and experimental results. However, the results appear to suggest that perhaps the differences are not attributable to the viscous effects. Potentially, the discrepancy may be related to the difference between the measured and calculated values of the net jet thrust, even though the former was corrected for various factors. These values are used, respectively, in calculating the experimental and computed amplification factor, K .

Figures 12 through 20 show the center of pressure shift as a function of angle of attack at Mach 2, 4.5, and 8 for each of the three bodies. In general, the predicted variation of ΔX_{CP} with angle of attack is in good agreement with the experimental data. The largest variation in ΔX_{CP} occurs at Mach 2. For all three bodies at Mach 2 and 4.5, ΔX_{CP} is positive, indicating a rearward shift in center of pressure. At Mach 8, ΔX_{CP} takes positive and negative values for negative and positive angles of attack, respectively.

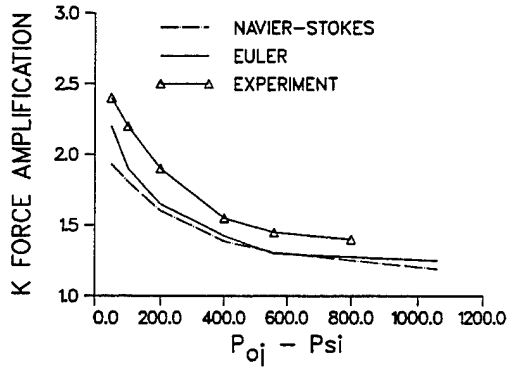


Figure 10. Force Amplification Factor as a Function of Jet Pressure, Mach 4.5, $\alpha = 0^\circ$, Straked Body.

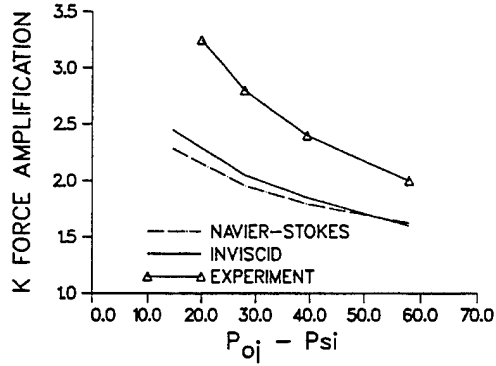


Figure 11. Force Amplification Factor as a Function of Jet Pressure, Mach 8.0, $\alpha = 0^\circ$, Straked Body.

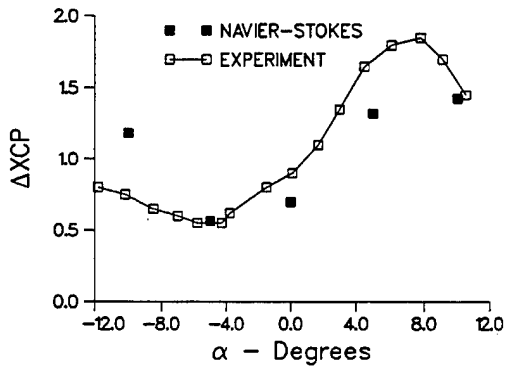


Figure 12. Center of Pressure Versus Angle of Attack, Mach 2, $P_{oj} = 27$ atm, Body Alone.

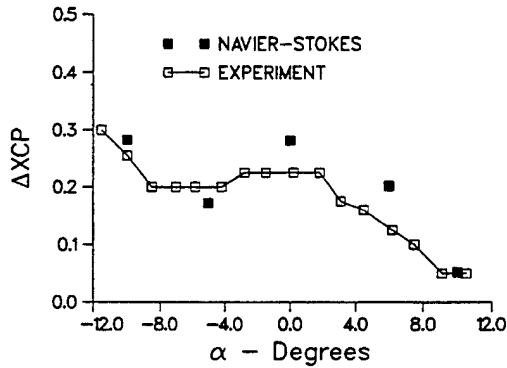


Figure 13. Center of Pressure Versus Angle of Attack, Mach 4.5, $P_{oj} = 38$ atm, Body Alone.

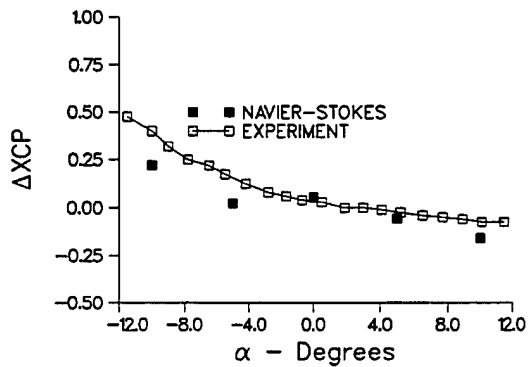


Figure 14. Center of Pressure Versus Angle of Attack, Mach 8, $P_{oj} = 1.9$ atm, Body Alone.

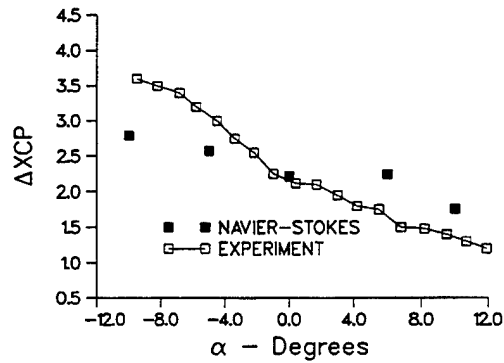


Figure 15. Center of Pressure Versus Angle of Attack, Mach 2, $P_{oj} = 27$ atm, Tail Fins.

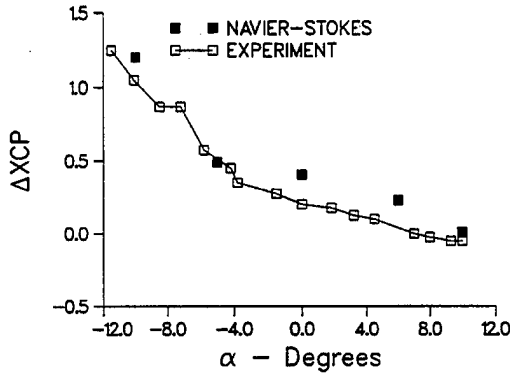


Figure 16. Center of Pressure Versus Angle of Attack, Mach 4.5, $P_0 = 38$ atm, Tail Fins.

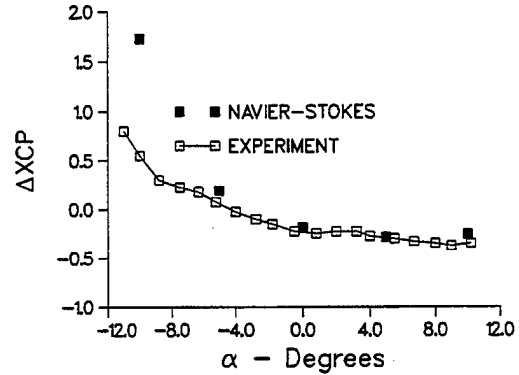


Figure 17. Center of Pressure Versus Angle of Attack, Mach 8, $P_0 = 1.9$ atm, Tail Fins.

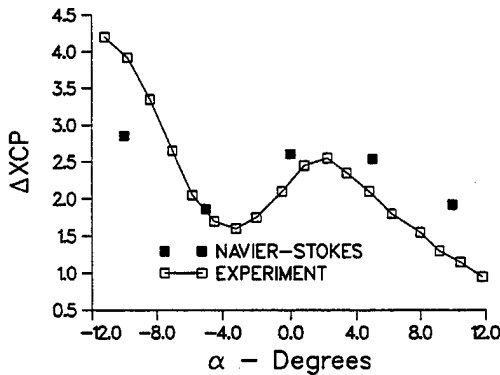


Figure 18. Center of Pressure Versus Angle of Attack, Mach 2, $P_0 = 27$ atm, Straked Body.

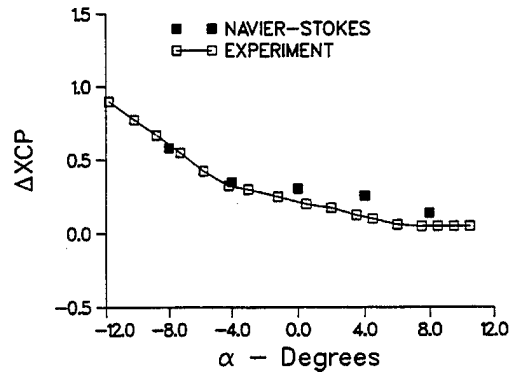


Figure 19. Center of Pressure Versus Angle of Attack, Mach 4.5, $P_0 = 38$ atm, Straked Body.

Figures 21 and 22 show the corresponding jet interaction moment as a function of angle of attack at Mach 4.5 and 8, respectively, for the straked body. At Mach 4.5, the Navier-Stokes and inviscid predictions are essentially equivalent and agree well with the experimental data. Here, there is an increasing trend with angle of attack for the interaction moment that is predicted by CFD and observed in the experiment. Although the increase in the moment is relatively small, it is attributable to the jet wake effects. At lower angles of attack, the jet wake effects interact with the rear of the vehicle much more strongly than they do at higher angles of attack. At Mach 8, the Navier-Stokes results appear to be in better agreement with the experimental data than do the inviscid results, although the moment is relatively small (ΔXCP at $\alpha = 0^\circ$ is about a quarter caliber).

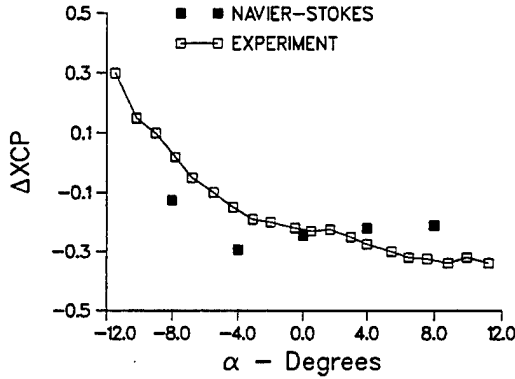


Figure 20. Center of Pressure Versus Angle of Attack, Mach 8, $P_0 = 1.9$ atm, Straked Body.

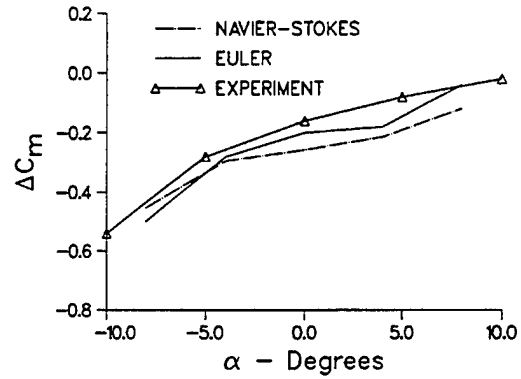


Figure 21. Jet Interaction Moment as a Function of Angle of Attack, $P_0 = 38$ atm, Straked Body.

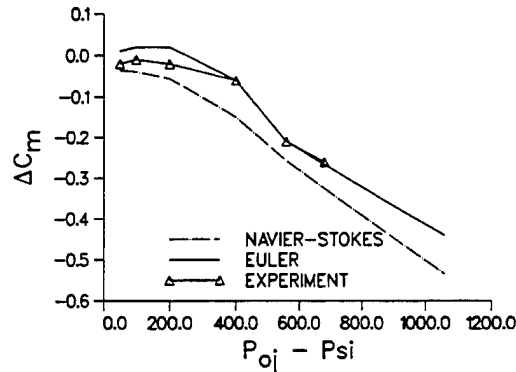


Figure 22. Jet Interaction Moment as a Function of Jet Pressure, Mach 4.5, $\alpha = 0^\circ$, Straked Body.

The Navier-Stokes computations were performed under the viscous assumption, which may account for the closer comparison than the Euler results. As indicated in Brandeis' results [5], these graphs show that at small angles of attack, the jet interaction's effects produce a nose-up pitching moment.

4. Scientific Visualization

Scientific visualization provides a methodology to explore, define, and present the results of computations generated on high performance, parallel computers. Through the use of real-time 3-D interactive exploration and animated depictions of their data, researchers are able to extrude and present previously unobservable information. The results of a visual analysis can be used to compare mach contours resulting from a computation with schlieren photographs from live experiments. Scientific visualization provides technical

innovations that present data in unique and nontraditional ways. Through these new techniques, more visual information is made available to the researcher, improving comprehension and providing new insight to the problem.

The computational results for this problem, which required 250 hours of CPU time to process, were analyzed and reported by a variety of 2-D and 3-D graphical techniques. The use of scientific visualization techniques was essential for analyzing a data set of this magnitude; for this particular problem, approximately 7.5 gigabytes of data, encompassing 236 time steps, were generated. The resulting visualization required the interactive display and manipulation of more than 1.5 million cells of data per time step. The ability to visualize and verify these results and share those findings with colleagues and customers was an invaluable part of the engineering process.

A commercially available scientific visualization package "EnSight™" was used to post-process the results of this computation. This package was able to visually display the time steps (236) of data that were generated as the computation converged to a steady state solution. EnSight™ uses many of the same parallel programming techniques that were used to generate the data, therefore taking full advantage of the multi-processing architecture of the visualization server to improve the efficiency and interactive response during the visual analysis process. Reducing 7.5 gigabytes of computed data into a single animation allowed for visual inspection of the evolution of the computation over time and provided real-time analysis of the jet-thruster phenomena.

Scientific visualization techniques were used to demonstrate the physical forces and interaction in and around the lateral jet thruster. This visual analysis clearly indicated the jet-on/jet-off state of the lateral jet thruster during the course of the computation. Also, the effects of the jet wake as it interacted with the aft-mounted fins of the vehicle could be visually analyzed. The use of pressure values to color-code the results of the 3-D analysis provided additional insight into the forces acting on the vehicle body, and the results of the jet thruster could be indicated.

5. Summary and Conclusions

A computational approach has been validated with experimental data for bodies with lateral control jets in supersonic flight at varying Mach numbers and angles of attack and for different jet stagnation pressures. The bodies include body-alone configurations, a body with aft-mounted tail fins, and a body with strakes. The results show significant interactions of the jet-induced flow field with the fin surfaces, which produce additional effects compared with the body alone. In

agreement with the experiment in some cases, the presence of lifting surfaces resulted in force and/or moment amplification of the jet interaction with the missile surfaces. The results indicate deamplification of the jet force at Mach 2 for all three bodies. Amplification of the jet force was also observed for high Mach numbers, particularly for the body with strakes. For the results examined here, there were only minor differences in the global force and moment predictions with viscous or inviscid techniques. This similarity indicates that the viscous effects are small for these configurations, especially in view of the large lifting surfaces that receive the pressure forces. Both techniques correctly predicted the dependence of the interaction parameters on angle of attack and jet pressure. The results indicate that for the purpose of overall design of configurations with jet force control, the inviscid methods may be both sufficient and expedient. Viscous computations are, however, imperative when the near field close to the jet is considered.

References

1. Brandeis, J., and J. Gill, "Experimental Investigation of Side-Jet Steering for Supersonic and Hypersonic Missiles," *Journal of Spacecraft and Rockets*, Vol. 33, No. 3, pp. 346-352, May-June 1996.
2. Spaid, F.W., and E.E. Zukoski, "A Study of the Interaction of Gaseous Jets from Transverse Slots with Supersonic External Flows," *AIAA Journal*, Vol. 6, No. 2, pp. 205-212, February 1968.
3. Gilman, R.G., "Control Jet Interaction Investigation," *Journal of Spacecraft and Rockets*, Vol. 8, No. 4, pp. 334-339, April 1971.
4. Spaid, F.W., "Two-Dimensional Jet Interaction Studies at Large Values of Reynolds and Mach Numbers," *AIAA Journal*, Vol. 13, No. 11, pp. 1430-1434, November 1975.
5. Brandeis, J., and J. Gill, "Experimental Investigation of Super- and Hypersonic Jet Interaction on Missile Configurations," *Journal of Spacecraft and Rockets*, Vol. 35, No. 3, May-June 1998.
6. McMaster, D.L., J.S. Shang, and W.C. Golbitz, "Supersonic, Transverse Jet from a Rotating Ogive Cylinder in a Hypersonic Flow," *Journal of Spacecraft and Rockets*, Vol. 26, No. 1, pp. 24-30, January-February 1989.
7. Chamberlain, R., "Calculation of Three-Dimensional Jet Interaction Flow Fields," AIAA Paper 90-2099, July 1990.
8. Hsieh, T., and A.B. Wardlaw, "Numerical Simulation of Cross Jets in Hypersonic Flow Over a Biconic Body," AIAA Paper 94-0165, January 1994.
9. Sahu, J., "Numerical Computations of Three Dimensional Jet Interaction Flow Fields," AIAA Paper 94-3521, August 1994.
10. Srivastava, B., "Aerodynamic Performance of Supersonic Missile Body- and Wing Tip-Mounted Lateral Jets," *Journal of Spacecraft and Rockets*, Vol. 35, No. 3, pp. 278-286, May-June 1998.
11. Graham, M.J., and P. Weinacht, "A Numerical Investigation of Supersonic Jet Interaction for Axisymmetric Bodies," *Journal of Spacecraft and Rockets*, Vol. 37, No. 5, pp. 675-683, September-October 2000.

12. Pulliam, T.H., and J.L. Steger, "On Implicit Finite-Difference Simulations of Three-Dimensional Flow," *AIAA Journal*, Vol. 18, No. 2, pp. 159-167, February 1982.
13. Baldwin, B.S., and H. Lomax, "Thin Layer Approximation and Algebraic Model for Separated Turbulent Flows," AIAA Paper 78-257, January 1978.
14. Cebeci, T., "Calculation of Compressible Turbulent Boundary Layers with Heat and Mass Transfer," AIAA Paper 70-741, June-July 1970.
15. Ying, S.X., J.L. Steger, L.B. Schiff, and D. Baganoff, "Numerical Simulation of Unsteady, Viscous, High-Angle-of-Attack Flows Using a Partially Flux-Split Algorithm," AIAA Paper 86-2179, August 1986.
16. Sahu, J., and J.L. Steger, "Numerical Simulation of Three-Dimensional Transonic Flows," *International Journal for Numerical Methods in Fluids*, Vol. 10, 1990, pp. 855-873.
17. Steger, J.L., and R.F. Warming, "Flux Vector Splitting of the Inviscid Gasdynamic Equations with Application to Finite-Difference Methods," *Journal of Computational Physics*, Vol. 40, 1981 pp. 263-293.
18. Steger, J.L., and P. Buning, "Developments in the Simulation of Compressible Inviscid and Viscous Flow on Supercomputers," NASA TM 86674, 1985.
19. Beam, R., and R.F. Warming, "An Implicit Factored Scheme for the Compressible Navier-Stokes Equations," *AIAA Journal*, Vol. 16, No. 4, 1978, pp.393-402.
20. Benek, J.A., T.L. Donegan, and N.E. Suhs, "Extended Chimera Grid embedding Scheme with Application to Viscous Flows," AIAA Paper No. 87-1126-CP, 1987.
21. Meakin, R.L., "Composite Overset Structured Grids," *CRC Handbook of Grid Generation*, CRC Press, Inc., Boca Raton, FL, 1997.
22. Anonymous, "INCA: 3D Multi-Zone Navier-Stokes Flow Analysis with Finite Rate Chemistry," *User's Manual*, Amtec Engineering, Inc., Bellevue, Washington, January 1992.
23. Anonymous, "GridPro/az3000 - User's Guide and Reference Manual," Program Development Corporation, 300 Hamilton Avenue, White Plains, New York, August 1994.

NO. OF
COPIES ORGANIZATION

1 ADMINISTRATOR
DEFENSE TECHNICAL INFO CTR
ATTN DTIC OCA
8725 JOHN J KINGMAN RD
STE 0944
FT BELVOIR VA 22060-6218

1 DIRECTOR
US ARMY RSCH LABORATORY
ATTN AMSRL CI AI R REC MGMT
2800 POWDER MILL RD
ADELPHI MD 20783-1197

1 DIRECTOR
US ARMY RSCH LABORATORY
ATTN AMSRL CI LL TECH LIB
2800 POWDER MILL RD
ADELPHI MD 207830-1197

1 DIRECTOR
US ARMY RSCH LABORATORY
ATTN AMSRL D D SMITH
2800 POWDER MILL RD
ADELPHI MD 20783-1197

1 AIR FORCE RSCH LABORATORY
ATTN ARFL/VAA DR J SHANG
BLDG 146B
2210 8TH ST
WPAFB OH 45433-7510

2 AIR FORCE RSCH LABORATORY
ATTN AFRL/MNAV G ABATE
G WINCHENBACH
101 W EGLIN BLVD STE 219
EGLIN AFB FL 32542-6810

2 CDR NAVAL SURF WARFARE CTR
WEAPONS SYSTEMS DEPT G04
ATTN DR FRANK MOORE
THOMAS HYMER
17320 DAHLGREN RD
DAHLGREN VA 22448-5150

1 DR WILLIAM REINECKE
INST FOR ADV TECHNOLOGY
THE UNIV OF TEXAS AT AUSTIN
4030-2 W BRAKER LN
AUSTIN TX 78759-5329

NO. OF
COPIES ORGANIZATION

4 CDR US ARMY TACOM ARDEC
ATTN AMSTE AR FSF T C NG
H HUDGINS B WONG
J GRAU
BLDG 382
PICATINNY ARSENAL NJ 07806-5000

1 CDR USAAMCOM
ATTN AMSAM RS SS
G LANDINGHAM
REDSTONE ARSENAL AL 35898-5252

2 CDR USAAMCOM
ATTN AMSAM RD SS AS E VAUGHN
D WASHINGTON
REDSTONE ARSENAL AL 35898-5252

1 CDR NSWC
CODE 420 DR A WARDLAW
INDIAN HEAD MD 20640-5035

1 USMA
THAYER HALL
ATTN MADN-MATH-MSCE
WEST POINT NY 10996-1786

1 MIT
TECH LIBRARY
77 MASSACHUSETTS AVE
CAMBRIDGE MA 02139

1 MISSISSIPPI STATE UNIV
ATTN PROF B SONI
ENG RES CTR RM 228
BOX 9627
MS STATE MS 39762

1 UNIV OF TEXAS
DEPT OF MECH ENGINEERING
ATTN DR D S DOLLING
AUSTIN TX 78712-1085

2 LOCKHEED MARTIN VOUGHT SYS
DEPT OF MECH ENGINEERING
PO BOX 65003 M/S EM 55
ATTN P A WOODEN
W B BROOKS
DALLAS TX 75265-0003

<u>NO. OF COPIES</u>	<u>ORGANIZATION</u>
2	ARROW TECH ASSOCIATES ATTN R WHYTE W HATHAWAY 1233 SHELBURNE RD SUITE D-8 SOUTH BURLINGTON VT 05403
1	OREGON STATE UNIV DEPT MECH ENGINEERING ATTN DR M COSTELLO CORVALLIS OR 97331
1	UNIV OF ILLINOIS AT URBANA CHAMPAIGN DEPT OF MECH & INDUS ENG ATTN DR J C DUTTON URBANA IL 61801
1	METACOMP TECHNOLOGIES INC ATTN S R CHAKRAVARTHY 650 HAMPSHIRE ROAD SUITE 200 WESTLAKE VILLAGE CA 91361-2510
1	LAWRENCE LIVERMORE NATL LAB ATTN DR M J GRAHAM PO BOX 808 LIVERMORE CA 94550
1	TETRA RSCH CORP ATTN DR R CHAMBERLAIN 2610 SPICEWOOD TR HUNTSVILLE AL 35811-2604
1	UNDER SECY OF THE ARMY 102 ARMY PENTAGON ATTN SAUS-OR DR D WILLARD WASHINGTON DC 20310-0102
1	UNDER SECY OF THE ARMY 102 ARMY PENTAGON ATTN ASA (ALT) DR H DUBIN WASHINGTON DC 20310-0102
	<u>ABERDEEN PROVING GROUND</u>
2	DIRECTOR US ARMY RSCH LABORATORY ATTN AMSRL CI LP (TECH LIB) BLDG 305 APG AA

<u>NO. OF COPIES</u>	<u>ORGANIZATION</u>
3	CDR US ARMY ARDEC FIRING TABLES BRANCH ATTN R LIESKE R EITMILLER F MIRABELLE BLDG 120
1	DIR USARL ATTN AMSRL CI H C NIETUBICZ BLDG 394
1	DIR USARL ATTN AMSRL CI HA R NOACK BLDG 394
1	DIR USARL ATTN AMSRL CI H W STUREK BLDG 328
2	DIR USARL ATTN AMSRL WM E M SCHMIDT D SMITH BLDG 4600
2	DIR USARL ATTN AMSRL WM B A W HORST JR W CIPEIELLA BLDG 4600
3	DIR USARL ATTN AMSRL WM BA D LYON F BRANDON T BROWN BLDG 4600
2	DIR USARL ATTN AMSRL WM BD B FORCH M NUSCA BLDG 4600
1	DIR USARL ATTN AMSRL WM BF J LACETERA BLDG 390

NO. OF
COPIES ORGANIZATION

18 DIR USARL
ATTN AMSRL WM BC
P PLOSTINS
M BUNDY
G COOPER
M DEL GUERCIO
J DESPIRITO
T ERLINE
J GARNER
B GUIDOS
K HEAVEY
J NEWILL
V OSKAY
J SAHU
K SOENCKSEN
D WEBB
P WEINACHT (3 CYS)
A ZIELINSKI
BLDG 390

ABSTRACT ONLY

1 DIRECTOR
US ARMY RSCH LABORATORY
ATTN AMSRL CI AP TECH PUB BR
2800 POWDER MILL RD
ADELPHI MD 20783-1197

INTENTIONALLY LEFT BLANK

REPORT DOCUMENTATION PAGE

Form Approved
OMB No. 0704-0188

Public reporting burden for this collection of information is estimated to average 1 hour per response, including the time for reviewing instructions, searching existing data sources, gathering and maintaining the data needed, and completing and reviewing the collection of information. Send comments regarding this burden estimate or any other aspect of this collection of information, including suggestions for reducing this burden, to Washington Headquarters Services, Directorate for Information Operations and Reports, 1215 Jefferson Davis Highway, Suite 1204, Arlington, VA 22202-4302, and to the Office of Management and Budget, Paperwork Reduction Project (0704-0188), Washington, DC 20503.

1. AGENCY USE ONLY (Leave blank)		2. REPORT DATE December 2000	3. REPORT TYPE AND DATES COVERED Final	
4. TITLE AND SUBTITLE A Numerical Investigation of Supersonic Jet Interaction for Finned Bodies			5. FUNDING NUMBERS PR: 1L162618AH80	
6. AUTHOR(S) Graham, M.J. (U.S. Military Academy); Weinacht, P. (ARL); Brandeis, J. (Rafael); Angelini, R. (ARL)				
7. PERFORMING ORGANIZATION NAME(S) AND ADDRESS(ES) U.S. Army Research Laboratory Weapons & Materials Research Directorate Aberdeen Proving Ground, MD 21005-5066			8. PERFORMING ORGANIZATION REPORT NUMBER	
9. SPONSORING/MONITORING AGENCY NAME(S) AND ADDRESS(ES) U.S. Army Research Laboratory Weapons & Materials Research Directorate Aberdeen Proving Ground, MD 21005-5066			10. SPONSORING/MONITORING AGENCY REPORT NUMBER ARL-TR-2312	
11. SUPPLEMENTARY NOTES				
12a. DISTRIBUTION/AVAILABILITY STATEMENT Approved for public release; distribution is unlimited.			12b. DISTRIBUTION CODE	
13. ABSTRACT (Maximum 200 words) <p>A detailed numerical investigation of the interaction between a lateral jet and the external flow has been performed for a variety of missile body geometries. These include non-finned axisymmetrical bodies and finned bodies with either strakes or aft-mounted tail fins. The computations were performed at Mach numbers 2, 4.5, and 8. To obtain the numerical results, both Reynolds-averaged Navier-Stokes and Euler techniques were applied. The computational results were compared with results from a previously published wind tunnel study that consisted primarily of global force and moment measurements. The results show significant interactions of the jet-induced flow field with the fin surfaces, which produce additional effects compared with the body alone. In agreement with the wind tunnel study, in some cases the presence of lifting surfaces resulted in force and/or moment amplification of the jet interaction with the missile surfaces. The results indicate deamplification of the jet force at Mach 2 for all three bodies. Amplification of the jet force was also observed for high Mach numbers, particularly for the body with strakes. For the results examined here, there were only minor differences in the global force and moment predictions when viscous or inviscid techniques were used. The dependence of the interaction parameters on angle of attack and jet pressure was well predicted by both methods. The numerical techniques showed good agreement with the experiments at supersonic Mach numbers but only fair agreement for the hypersonic, Mach = 8 case.</p>				
14. SUBJECT TERMS computational fluid dynamics lateral jet			15. NUMBER OF PAGES 30	16. PRICE CODE
17. SECURITY CLASSIFICATION OF REPORT Unclassified	18. SECURITY CLASSIFICATION OF THIS PAGE Unclassified	19. SECURITY CLASSIFICATION OF ABSTRACT Unclassified	20. LIMITATION OF ABSTRACT	